

On the Sensitivity of Bevelled and Conical Coaxial Needle Probes for Dielectric Spectroscopy

Hossein Asilian Bidgoli¹, Nicola Schieda², and Carlos Rossa¹

Abstract—Dielectric spectroscopy measures the permittivity of a material in a wide frequency band for analysis and characterisation with many applications in biomedical engineering. It is typically performed by measuring the reflection coefficient of the material under test using an open flat-ended coaxial probe. However, probes with a flat end cannot cut through biological tissues and thus, can only be deployed for *ex-vivo* measurements. Bevelled and conical-ended coaxial probes can overcome this limitation as they can be integrated into existing surgical tools for *in-vivo* measurements. The geometry of the probe strongly affects the measurement accuracy and this effect must be modelled precisely before deployment. Although there has been significant research using flat-ended probes, there is very limited research investigating other probe geometries. In this paper, a closed-form model of a bevelled and a conical end coaxial probe is presented for the first time. The model is based on the analytical solution of aperture admittance. The accuracy of the model is validated using both simulation and experimental results with a relative error of less than 1% for a wide range of permittivity values and frequencies. Using the obtained model, the sensitivity of conical and bevelled probes is analysed and compared. The results indicate that bevelled probes have a higher sensitivity than conical probes for tissue measurement and thus are the preferable probe geometry for *in-vivo* deployment.

Index Terms—dielectric spectroscopy, bevelled coaxial probe, conical coaxial probe, permittivity measurement, *in-vivo* measurement, model optimization, open-ended coaxial probe, sensitivity, tissue measurement

I. INTRODUCTION

THE permittivity of biological tissue governs the interaction of electromagnetic fields with organizations at the cellular, molecular, and ionic levels, and is a strong biomarker for tissue identification. Dielectric spectroscopy is a technique used to measure the dielectric properties of a medium, including its permittivity, as a function of frequency. Permittivity tissue characterization has been done in radio frequency (RF), microwave, and more recently, in the millimetre-wave frequency band [1]–[6]. An important application of permittivity characterization is cancer detection. In fact, it is possible to differentiate malignant from benign tissue based on the tissue’s permittivity in the range of 10 Hz to 20 GHz [3], [7]–[9].

The most convenient method for determining the permittivity of a biological tissue is to subject it to an electromagnetic field and quantify its reflection coefficient, i.e., a parameter that describes how much of the electromagnetic field is reflected by the tissue [10]. Electromagnetic energy is applied to a material under test (MUT) using a transmission line. The injected energy is radiated, absorbed, or reflected. The reflection coefficient is the ratio of reflected energy to the transmitted energy through the transmission line at the contact plane of the MUT. The reflection coefficient depends on the permittivity of the material, and it can be measured by a vector network analyzer (VNA). Amongst the various type of transmission lines such as rectangular or circular waveguides, coaxial lines have the advantage of widening the range of frequencies at which measurements can be taken [11].

Different methods have been proposed to extract the permittivity values from the reflection coefficient. For example, a lumped equivalent circuit model of the MUT can be used, but a single set of model parameters is generally not able to describe the measured reflection coefficient across the entire frequency band that the probe covers [12]. Analytical solutions for the aperture admittance of an open-ended coaxial cable that radiates into an unbounded material have also been proposed. The measured reflection coefficient is fed to an iterative model to extract the permittivity values [11]. These methods are the basis of many commercial open-ended coaxial probes designed for measuring the permittivity of a variety of materials. Commercial probes typically take the form of coaxial cables with a flat end. Such a simple geometry, and the analogy that can be established with a transmission line opening to an infinite ground plane, is easier to model and analyse than more complex geometries [13]–[15].

A critical limitation of using flat open-ended coaxial probes is that they cannot be used for biological tissue characterization. Flat open-ended coaxial probes cannot cut through tissue, and therefore they cannot be easily integrated into surgical tools for *in-vivo* deployment, such as in biopsy needles and drainage catheters. All measurements performed with flat-ended probes must be conducted using *ex-vivo* excised tissue. *In-vivo* measurements may be more useful, especially if real-time feedback can be provided to guide biopsy procedures and focal treatment such as ablation [16]. A solution to this problem is to consider probes having a bevelled or conical coaxial end that can cut through tissue as the probe is inserted and steered towards a point of interest. This type of probe can then be integrated into diagnostic or treatment tools for *in-vivo* feedback about the characteristics of the tissue in contact with the probe’s tip. As a consequence of its sharp geometry, an

¹H. Asilian and C. Rossa are with the Department of Systems and Computer Engineering, Carleton University, Ottawa, ON, Canada

²N. Schieda is with the Department of Radiology, Radiation Oncology and Medical Physics, University of Ottawa, Ottawa, ON, Canada

This research is supported by the Canadian Cancer Society and the Canadian Institutes of Health Research (grant #944486).

Cette recherche est appuyée par la Société canadienne du cancer et les instituts de recherche en santé du Canada (subvention no 944486).

important benefit of using bevelled or conical-shaped probes is the decreased chance of trapping air between the probe's tip and the tissue.

Although many different models have been proposed to describe the aperture admittance of flat open-ended coaxial probes, there is a critical gap in the literature with regard to bevelled and conical open-ended coaxial probes. In fact, the probe's own geometry strongly affects the measured field reflected from the tissue. Therefore the effect of the probe's diameter and the bevel or conical cut angle on the probe's accuracy and sensitivity must be thoroughly investigated. Accuracy defines how well the probe can extract the true relative permittivity properties of the tissue, while sensitivity corresponds to its ability to detect small variations in the relative permittivity characteristics of the tissue [17]. More specifically, the sensitivity can be defined as the relative change in the measured reflection coefficient with respect to the relative change in permittivity. Sensitivity thus defines accuracy [18].

The development of a new probe for *in-vivo* permittivity tissue characterization requires: (1) An accurate model of the probe's admittance to extract the tissue's permittivity properties from the measured reflection coefficient; and (2) that the probe's sensitivity be quantified for different geometries to guide the choice of the optimal probe type.

This paper presents a broadband model of aperture admittance of an open-ended coaxial probe with bevelled and conical ends. First, in Section II an analytical model of the aperture admittance is derived for a generic open-ended probe. A Taylor series expansion is used to simplify the equations describing the admittance as a function of a series of geometry-specific coefficients. A procedure for obtaining these model coefficients is introduced in Section III. This is achieved by simulating different probe geometries in Ansys HFSS and using the data to find the model parameters. Experimental validation of the model using two probe geometries is presented in section IV. In Section V the model is used to quantify and compare the sensitivity of different probe geometries. Recommendations for the optimization the probe geometry and the consistency of the obtained results with previous work are also discussed. Finally, Section VI summarizes the main conclusions of this paper. To the best of the author's knowledge, such a comprehensive analysis for conical and bevelled end probes designed for *in-vivo* measurements has not been presented before.

II. ADMITTANCE MODEL OF A COAXIAL PROBE

Consider a coaxial probe with inner and outer radii a and b , respectively, filled with a lossless homogeneous dielectric having a relative permittivity ϵ_c . The tip of the probe is inserted into a tissue having a complex relative permittivity $\epsilon_m = \epsilon_r - j\frac{\sigma}{\omega\epsilon_0}$, where ϵ_r is the relative permittivity, σ is the conductivity, ω is the angular frequency, and ϵ_0 is the vacuum permittivity, as shown in Fig. 1(a). The probe can be terminated with either a flat, bevelled, or conical end. The cut angle α is the complementary angle between the probe's longitudinal axis and the tip's bevel or conical surface, see Fig. 1(b) and 1(c), respectively.

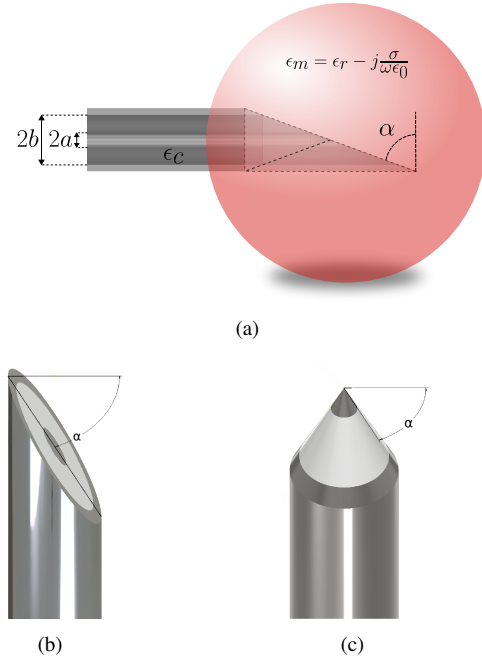


Fig. 1. (a) Geometry of flat, bevelled and conical open-ended coaxial probe filled with a dielectric having a relative permittivity ϵ_c and inner and outer radii a and b , respectively, immersed into the MUT with complex relative permittivity ϵ_m . (b) bevelled and (c) conical coaxial probe geometries with a cut angle α .

The normalized aperture admittance at the open-ended surface of this coaxial probe in terms of the dominant mode reflection coefficient (Γ) can be defined as:

$$Y_s = \frac{1 - \Gamma}{1 + \Gamma} \quad (1)$$

The coaxial line can support transverse electric (TE) and transverse magnetic (TM) wave propagation modes in addition to the transverse electromagnetic (TEM) mode. In practice, the TE and TM modes only have a reactive effect near the line's aperture and can be neglected elsewhere. In fact, the principal TEM can be considered the dominant mode for small cut angles (α) in the bevelled and conical geometries [19]. This assumption is correct if the frequency is well below the cut-off frequency of dominant TE or TM modes [20]. By matching the radiated fields of the aperture to the TEM of the coaxial line, the normalized admittance Y_s , in terms of the electric and magnetic field of the aperture (assuming radial symmetry), can be expressed as [19]:

$$Y_s = \frac{jk_m^2}{2\pi k_c} \times \frac{\int H_s \left(\int M_e \frac{e^{-jk_m R_e}}{R_e} ds' + \int M_i \frac{e^{-jk_m R_i}}{R_i} ds'' \right) ds}{\int E_s H_s ds} \quad (2)$$

where

$$k_c = \omega \sqrt{\epsilon_c \epsilon_0 \mu_0}$$

$$k_m = \omega \sqrt{\epsilon_m \epsilon_0 \mu_0}$$

and E_s and H_s are the surface tangential electric and magnetic field of the probe aperture respectively, M_e is the equivalent magnetic current source and M_i is the imaginary magnetic current source. R_e and R_i are the distances between the point where the inner and outer integrals are calculated in (2). Also, s and s' are the aperture surface, and s'' is the surface on which the imaginary magnetic current flows.

For a flat open-ended probe, that is, $\alpha = 0^\circ$ in Fig. 1(a), both magnetic current sources (M_e and M_i) are equal to E_s based on Huygens's principle and image theory. However, for bevelled and conical geometries these currents cannot be determined analytically since the two exponential terms within the integrals in (2) are concurrently dependent on the probe geometry and medium characteristics. The effect of the probe's geometry on the admittance is therefore not explicitly known.

As suggested in [21], the integrals in (2) can be made independent of the medium characteristics through a Taylor series expansion of its exponential terms. To provide a fast computation of the normalized aperture admittance using the expansion, (2) can be rewritten as:

$$Y_s = \frac{k_m^2}{2\pi k_c} \left[j \left(I_0 - \frac{k_m^2}{2} I_2 + \frac{k_m^4}{24} I_4 - \dots \right) - \left(k_m I_1 - \frac{k_m^3}{6} I_3 + \frac{k_m^5}{120} I_5 - \dots \right) \right] \quad (3)$$

where

$$I_n = \frac{\int H_s \left(\int M_e R_e^{n-1} ds' + \int M_i R_i^{n-1} ds'' \right) ds}{\int E_s H_s ds} \quad (4)$$

The terms I_n in the above equation, henceforward referred to as the probe's coefficient, are independent of the medium characteristics and solely a function of the geometry of the probe. These coefficients need to be calculated once for every probe geometry. Even though the analytical calculation of these coefficients is possible for simple geometries, an optimization method is required to include the effect of higher order modes and eliminate the infinite ground plane assumption [21]. The probe's coefficients can be identified by fitting the aperture admittance model (2) to some known aperture admittance obtained from experimental evaluation or simulations.

III. CALCULATING THE PROBE'S COEFFICIENTS

In this paper, the probe's coefficients are identified through model fitting using simulated data obtained from multiple materials and frequencies. Simulation is performed in Ansys HFSS. Subsequently, the model is validated in a different range of frequencies than that used for model fitting, and also experimentally in Section IV.

A. Data generation for model fitting

Fig. 2 shows a 3D drawing of a flat coaxial probe in a MUT in the simulation environment implemented in Ansys. Three different coaxial probe geometries are simulated i.e.,

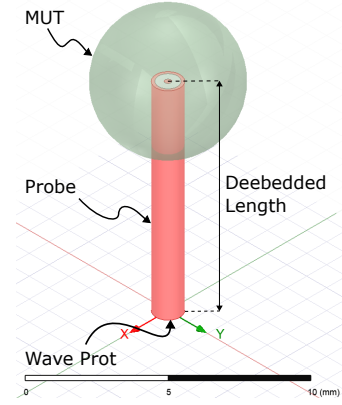


Fig. 2. Full-wave simulation of a flat open-ended coaxial probe inside the MUT (green sphere) in Ansys HFSS. Bevelled and coaxial geometries are also simulated, see Fig. 1(b) and 1(c).

the flat, a bevelled, and a conical shape. The latter two are simulated using two different cut angles, i.e., $\alpha = 60^\circ$ and $\alpha = 70^\circ$. These angles are chosen to match the cut angles of commercially available surgical and biopsy needles [22], [23]. The coaxial line dimension is a standard 50- Ω Teflon-filled cable with an external diameter of 1.15 mm, a dielectric radius of $b = 0.43$ mm and an inner conductor radius of $a = 0.14$ mm. The diameter of MUT is 5 mm, which is much larger than the sample zone in which the electromagnetic field penetrates [24]. To convert the simulated reflection coefficient to the aperture-plane reflection coefficient, the length of the probe's inner conductor is de-embedded from the simulation results.

Simulation is performed at two frequencies, i.e., 1 and 10 GHz. The permittivity values used for model identification are chosen to be within the range of biological tissues [1]–[5]. The relative permittivity of the MUT ranges from $1 \leq \epsilon_r \leq 100$ with increments of 5, while its conductivity ranges from $0 \text{ S/m} \leq \sigma \leq 100 \text{ S/m}$ in increments of 5 S/m. This amounts to 441 unique MUT and 882 simulations in total. Once the reflection coefficients are obtained, the normalized aperture admittance can be computed using (1) for every combination of (ϵ_r, σ) at each frequency.

B. Model fitting

The objective is to determine the probe's coefficients I_n so as to minimize the relative error between the admittance calculated using the model (Y_{model}) and the admittance obtained through the simulation (Y_{sim}), i.e.,

$$\text{Error} = \frac{1}{p} \sum_{i=1}^p \left| \frac{Y_{sim,i} - Y_{model}(I_n)_i}{Y_{sim,i}} \right| \quad (5)$$

where p is the number of simulations used. As the values of admittance vary significantly, the error is evaluated relative to the magnitude of the admittance.

An initial value for the coefficients can be obtained using the least square method (LSTSQ), which is built by the GELSD

TABLE I
RELATIVE MODEL FITTING ERROR

Method	Probe type				
	flat $\alpha = 0^\circ$	bevelled $\alpha = 60^\circ$	bevelled $\alpha = 70^\circ$	conical $\alpha = 60^\circ$	conical $\alpha = 70^\circ$
LSTSQ	4.1%	5.0%	7.2%	6.5%	8.9%
ADAM	0.4%	0.9%	0.8%	0.6%	2.7%

TABLE II
PROBE COEFFICIENTS FOR DIFFERENT GEOMETRIES

	Probe type				
	flat $\alpha = 0^\circ$	bevelled $\alpha = 60^\circ$	bevelled $\alpha = 70^\circ$	Conical $\alpha = 60^\circ$	Conical $\alpha = 70^\circ$
I_0	7.38×10^{-4}	1.10×10^{-3}	1.41×10^{-3}	1.40×10^{-3}	1.76×10^{-3}
I_1	-8.74×10^{-9}	3.81×10^{-9}	2.60×10^{-9}	-1.68×10^{-7}	-4.66×10^{-7}
I_2	-1.30×10^{-11}	-5.74×10^{-11}	-7.27×10^{-11}	-5.38×10^{-11}	7.14×10^{-11}
I_3	1.08×10^{-15}	6.48×10^{-14}	1.10×10^{-13}	-1.64×10^{-13}	-2.29×10^{-13}
I_4	3.58×10^{-18}	-3.59×10^{-17}	-3.75×10^{-17}	-1.78×10^{-16}	-3.71×10^{-16}
I_5	1.30×10^{-21}	1.80×10^{-20}	8.02×10^{-21}	1.18×10^{-19}	3.14×10^{-19}

routine from LAPACK package [25]. The LSTSQ method calculates the vector x such that it minimizes $\|b - Ax\|_2$ where:

$$b = [Y_{sim,1} \quad Y_{sim,2} \quad \cdots \quad Y_{sim,i}]^T \quad (6)$$

$$A = \frac{1}{2\pi k_c} \begin{bmatrix} k_{m,1}^2 & jk_{m,1}^3 & \cdots & jk_{m,1}^{n+2} \\ k_{m,2}^2 & jk_{m,2}^3 & \cdots & jk_{m,2}^{n+2} \\ \vdots & \vdots & \ddots & \vdots \\ k_{m,p}^2 & jk_{m,p}^3 & \cdots & jk_{m,p}^{n+2} \end{bmatrix}, \quad (7)$$

$$(8)$$

and vector x contains the probe's coefficients:

$$x = [I_0 \quad I_1 \quad \cdots \quad I_n]^T \quad (9)$$

The LSTSQ method is fast and does not need an initial guess. However, convergence to a global minimum is not guaranteed. To further reduce the fitting error, the result of the LSTSQ method is normalized and fed to an optimization method, in this case, the adaptive moment estimation method (Adam) is used [26]. This algorithm is a stochastic gradient descent method based on adaptive estimation of first-order and second-order moments. The optimization procedure is summarized in Fig. 3.

C. Optimization Results

Table I shows the residual fitting error after the least square and Adam algorithms. An error of less than 1% is obtained with $n = 6$ for all geometries except for the conical probe with $\alpha = 70^\circ$, for which the error is 2.7%. The calculated probe's coefficients are shown in Table II.

Once the probe's coefficients are calculated, they can be used to estimate the probe's admittance at other frequencies. The same set of simulations is then conducted at 0.5, 5, and 15 GHz. The model is validated by comparing the simulated admittance with the one obtained from the model using the parameters listed in Table II. The relative error in the (ϵ_r, σ) plane is shown in Fig. 4 for all geometries and newly simulated

TABLE III
TOTAL RELATIVE MODEL ERROR AT 0.5, 5, AND 15 GHz

Frequency	Probe Type				
	flat $\alpha = 0^\circ$	bevelled $\alpha = 60^\circ$	bevelled $\alpha = 70^\circ$	conical $\alpha = 60^\circ$	conical $\alpha = 70^\circ$
0.5 GHz	1.2%	1.6%	1.6%	1.4%	1.8%
5 GHz	1.4%	1.4%	1.5%	1.3%	2.8%
15 GHz	1.6%	1.9%	4.6%	7.5%	9.2%

frequencies. The total error for each geometry and frequency is summarized in Table III. As the results show, the model performs well for frequencies below the highest frequency used for model fitting, in this case, 10 GHz. The average error at 0.5 and 5 GHz are less than 1.8% and 2.8% respectively, and the maximum error is 3.8% and 5% respectively. It can also be seen that when the frequency is higher than the maximum frequency used for model fitting, the model may not perform well and can reach an error of 20% at 15 GHz for example; see Fig. 4(m)-(o). This is because the higher-order modes present at high frequencies are not captured when the model is fitted at a lower frequency. Consequently, it is recommended to use at least one frequency higher than the operating frequency for training the model.

Having the probe's coefficients, the proposed model can be used to extract the permittivity of the tissue at a given frequency. This is done by finding the roots of $Y_s(k_m) = Y_{measured}$ in (3), and then choosing the roots that satisfy the physical constraint, that is $\epsilon_m > 1$ and $\sigma > 0$ S/m. The measured normalized admittance $Y_{measured}$ can also be calculated using the measured reflection coefficient in (1).

IV. EXPERIMENTAL VALIDATION

To validate the proposed model experimentally, two probes were fabricated: one having a flat end, and another one with a bevel angle of 60° . The probes are connected to a vector network analyzer to measure the reflection coefficient of a MUT with known dielectric properties. The frequency ranges from 0.5 GHz to 10 GHz with intervals of 50 MHz. From the measured reflection coefficients, the dielectric properties of the MUT are then estimated using the model presented earlier, and the results are compared to the known permittivity and conductivity of the MUT.

The measured reflection coefficients can not be directly processed as the raw measurements include systematic measurement errors. To remove these errors and map the measured reflection coefficient to the aperture/material interface, calibration of the system is needed. In this paper, the same calibration method discussed in [21] is used. The errors include the systematic errors of directivity (e_d), frequency response (e_r), and source match (e_s). The relation between these errors, the actual reflection coefficient (Γ_a) and the the measured reflection coefficient (Γ_m) is given by:

$$\Gamma_a = e_d + \frac{e_r \Gamma_m}{1 - e_s \Gamma_m} \quad (10)$$

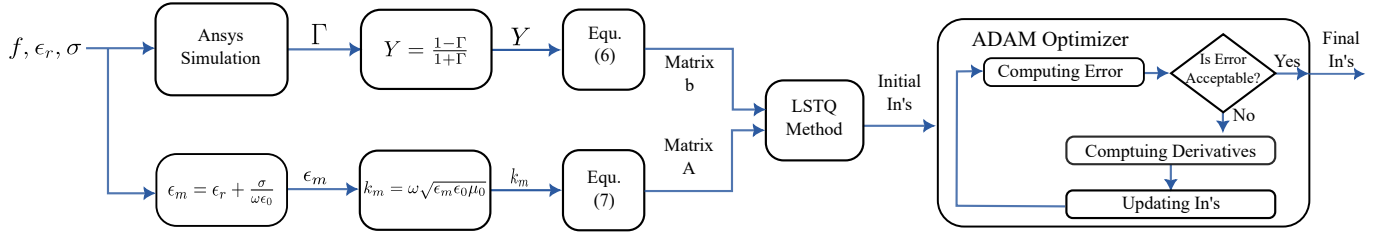


Fig. 3. Block diagram of the optimization algorithm. Calculation of the probe's coefficients using simulation results.

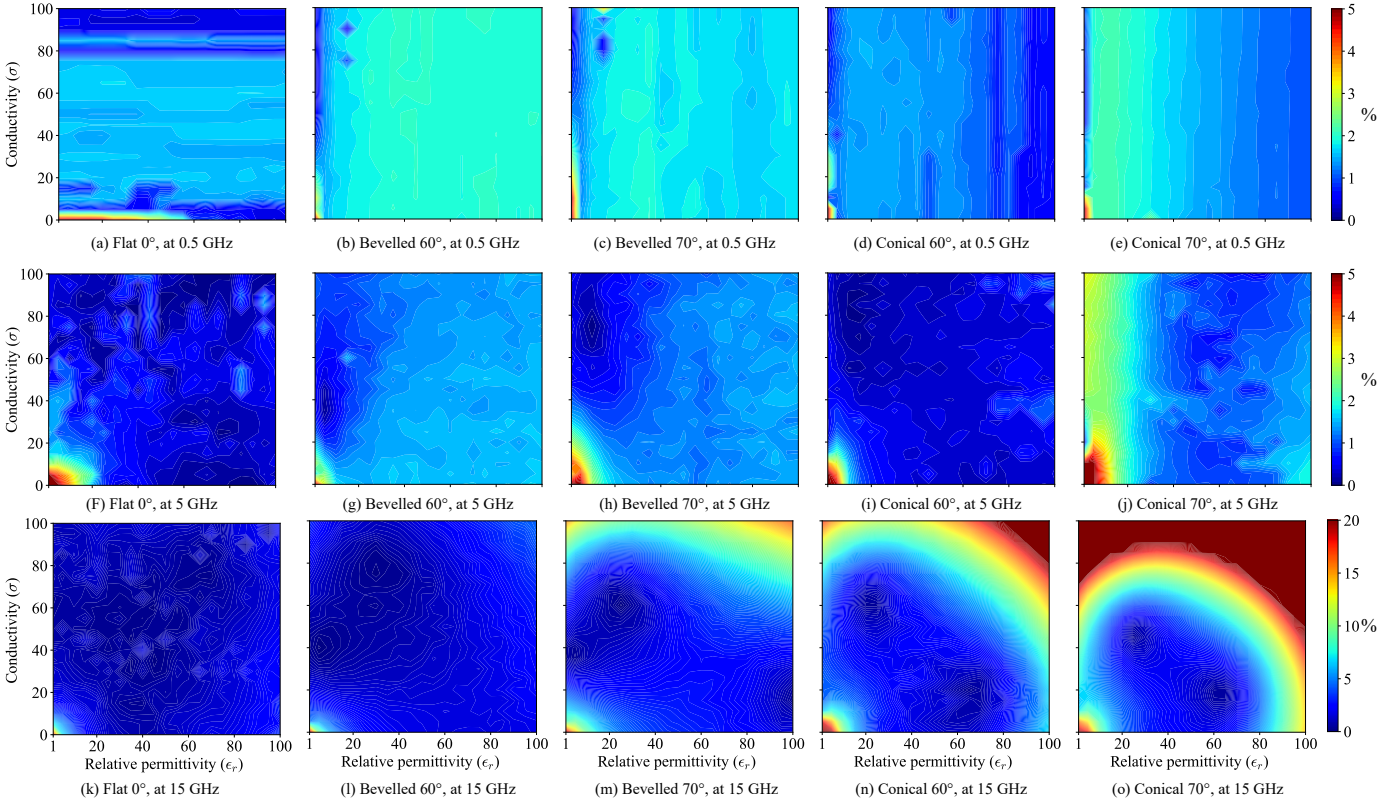


Fig. 4. Model relative error in (ϵ_r, σ) plane for different geometries at validation frequencies. Error is shown in percentage (%).

The three coefficients in (10) can be determined once the reflection coefficient of three calibration standards are known. Air, methanol, and short circuit are the three common calibration standards used to infer these coefficients for coaxial probes. The actual reflection coefficient (Γ_a) of the calibration standards can be determined using simulation as discussed in Section III. The complex permittivity values of the calibration standards are obtained by the Cole-Cole equation:

$$\epsilon_m = \epsilon_\infty + \frac{\epsilon_s - \epsilon_\infty}{1 + (j\omega\tau)^{1-\alpha}} \quad (11)$$

where ϵ_∞ is the optical permittivity, ϵ_s is the static permittivity, τ is the relaxation time, α is the distribution parameter. The Cole-Cole parameter of the reference liquids can be found in [27], [28]. For short circuit calibration, the tip of the probe is submerged in liquid gallium. Having all the actual reflection coefficients (Γ_a) and the measured reflection coefficient (Γ_m) of the calibration standards, a system of three equations can be

obtained. The calibration errors (i.e., the coefficients in (10)) are the solution to this system of equations.

After calculating the calibration errors, the reflection coefficient can be determined by:

$$\Gamma_a = \frac{\Gamma_m - \epsilon_d}{\epsilon_s(\Gamma_m - \epsilon_d) + \epsilon_r} \quad (12)$$

Having the actual reflection coefficient of a material, the relative permittivity is calculated by interactively solving (3). The actual normalized aperture admittance can be calculated using (1). For every measurement frequency, the measured admittance is equated to (3), and the root of the resulting equation corresponds to k_m . The complex relative permittivity (ϵ_m) then is:

$$\epsilon_m = \frac{k_m^2}{\omega^2 \epsilon_0 \mu_0} \quad (13)$$

Based on physical considerations, the root must lead to a complex relative permittivity with a real part larger than 1,

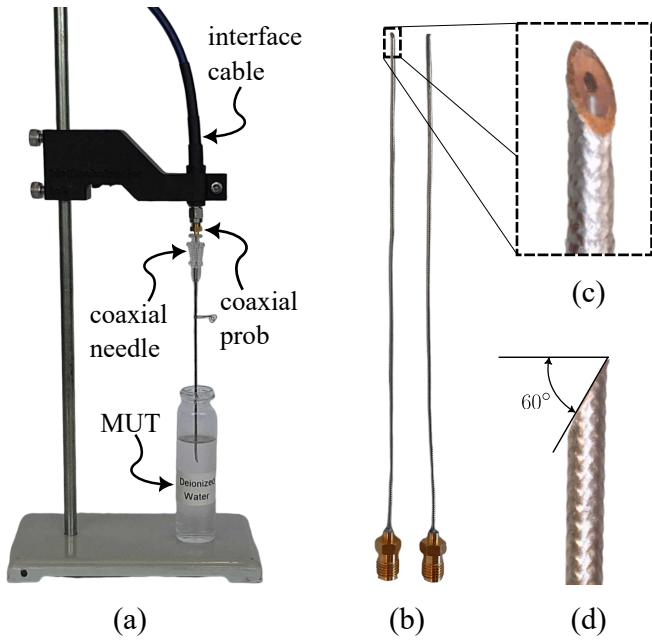


Fig. 5. Reflection coefficient measurement setup and tools. (a) measurement setup, (b) coaxial probes, (c) perspective and (d) side views of the 60° bevelled probe.

and an imaginary part larger than 0 ($\epsilon_r > 1$, $\frac{\sigma}{\omega\epsilon_0} > 0$). In this work, two roots satisfy this condition. They have almost identical magnitudes (less than 1% difference in ϵ_m) but with opposite sign.

The permittivity of the water at room temperature (25 °C) is calculated using the above procedure using the flat and the 60° bevelled probes. Fig 5 shows the measurement setup. The measured and calibrated (actual) reflection coefficients are illustrated in Fig. 6. Fig. 7, shows good consistency between the Cole-Cole model of water and the measured values. The fluctuation in the results, especially in higher frequencies, mostly resulted from calibration errors. An interpolation technique could mitigate this error.

V. SENSITIVITY ANALYSIS

In addition to extracting permittivity values from reflection measurements, a significant advantage of having a closed-form solution for aperture admittance is that it allows one to quantify the sensitivity of the probe with different geometries. The sensitivity of a coaxial probe can be defined as the relative change in measured reflection coefficient (Γ) with respect to a relative change in relative permittivity (ϵ_r). Measurements from a probe with low sensitivity will be prone to error. Therefore, the proper probe geometry with an acceptable sensitivity range must be chosen for a specific material. The sensitivity of a coaxial probe also depends on other variables, such as the frequency and temperature, but their effect is of limited importance and is not considered here [29].

The sensitivity of a coaxial probe with respect to relative permittivity can be defined as follows [29]:

$$S_{\epsilon_m}^{\Gamma} = \left| \frac{\epsilon_m}{\Gamma} \frac{\partial \Gamma}{\partial \epsilon_m} \right|. \quad (14)$$

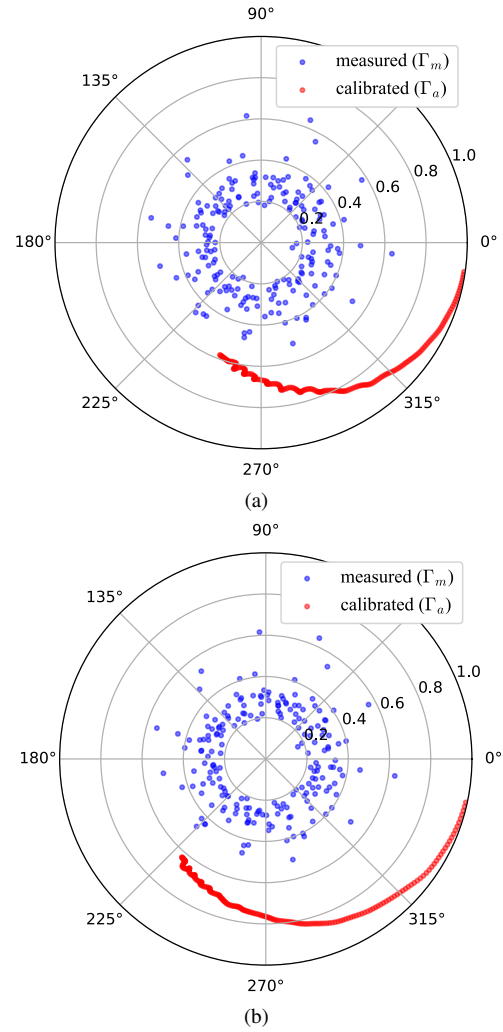


Fig. 6. Measured reflection coefficient of water from 0.5 to 10 GHz at 25°C before and after calibration using a flat (a) and a 60° bevelled probe (b).

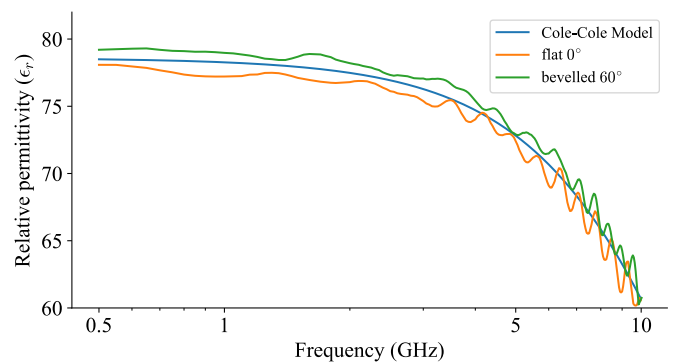


Fig. 7. Comparison of relative permittivity measurement of water at 25°C using both flat and bevelled 60°. Cole-Cole model for water is also included.

using the chain rule, the sensitivity can be expressed as the partial derivative of the aperture admittance:

$$S_{\epsilon_m}^{\Gamma} = \left| \frac{\epsilon_m}{\Gamma} \frac{\partial \Gamma}{\partial Y_m} \frac{\partial Y_m}{\partial \epsilon_m} \right| \quad (15)$$

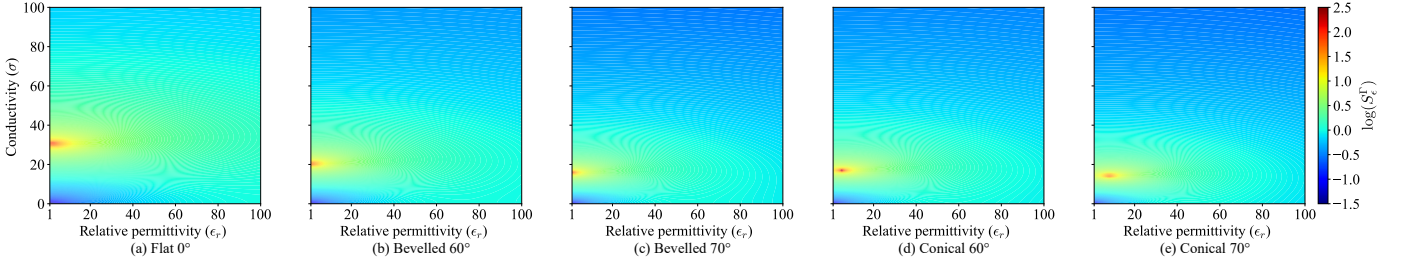


Fig. 8. Sensitivity of the flat, bevelled, and conical probe with $a=0.14$ mm, $b=0.43$ mm at 5 GHz in logarithmic scale. Peaks of sensitivity for (a)-(e) are located at (2.2, 30.6), (1, 20.4), (1, 15.8), (5.1, 17) and (8, 14.3), respectively.

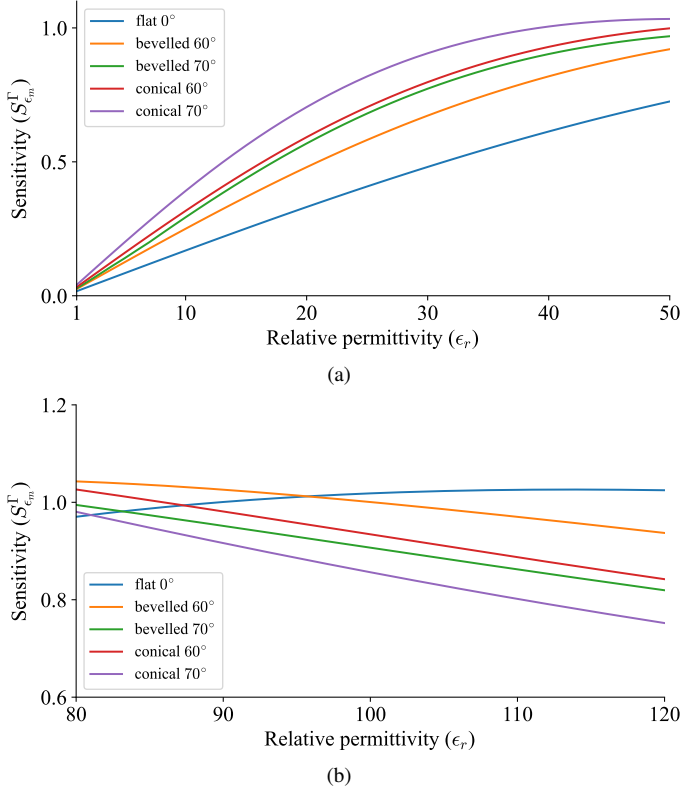


Fig. 9. Sensitivity of flat, bevelled and conical probe with $a = 0.14$ mm and $b = 0.43$ mm at 5 GHz. (a) $\sigma = 0$ S/m and (b) $\sigma = 5$ S/m.

replacing the derivative of (1) in (15):

$$S_{\epsilon_m}^{\Gamma} = \left| \epsilon_m \frac{1+Y}{1-Y} \frac{-2}{(1+Y)^2} \frac{\partial Y}{\partial \epsilon_m} \right| \quad (16)$$

simplifying the equation above results in:

$$S_{\epsilon_m}^{\Gamma} = \left| \frac{2\epsilon_m}{(1-Y^2)} \frac{\partial Y}{\partial \epsilon_m} \right| \quad (17)$$

again using the chain rule, one may define the sensitivity as a functional derivative of aperture admittance with respect to k_m as:

$$S_{\epsilon_m}^{\Gamma} = \left| \frac{2\epsilon_m}{(1-Y^2)} \frac{\partial Y}{\partial k_m} \frac{\partial k_m}{\partial \epsilon_m} \right| \quad (18)$$

Replacing $\partial k_m / \partial \epsilon_m$ in (18) yields:

$$S_{\epsilon_m}^{\Gamma} = \left| \frac{2\epsilon_m}{(1-Y^2)} \frac{\partial Y}{\partial k_m} \frac{\omega \sqrt{\mu_0 \epsilon_0}}{2\sqrt{\epsilon_m}} \right| \quad (19)$$

and by further replacing the derivative of (3) with respect to k_m into (19), one obtains:

$$S_{\epsilon_m}^{\Gamma} = \left| \frac{\omega \sqrt{\mu_0 \epsilon_0 \epsilon_m}}{\left(1 - \frac{1}{4\pi^2 k_c^2} \sum_{n=0}^5 \frac{(-1)^{n+1}}{(n!)^2} k_m^{n+2} I_n^2\right)} \right| \quad (20)$$

$$\left| \frac{1}{2\pi k_c} \sum_{n=0}^5 \frac{j^{n+1}}{n!} (n+2) k_m^{n+1} I_n \right|$$

Finally, simplifying the equation above gives the sensitivity as:

$$S_{\epsilon_m}^{\Gamma} = \left| \frac{2\pi k_c \sum_{n=0}^5 \frac{j^{n+1}}{n!} (n+2) (\omega \sqrt{\mu_0 \epsilon_0 \epsilon_m})^{n+2} I_n}{4\pi^2 k_c^2 + \sum_{n=0}^5 \frac{(-1)^n}{(n!)^2} (\omega^2 \mu_0 \epsilon_0 \epsilon_m)^{n+2} I_n^2} \right| \quad (21)$$

Close scrutiny of (21) reveals that the sensitivity is a function of frequency, permittivity, and the probe's coefficients. Fig. 8 shows the sensitivity of each probe geometry in the (ϵ_r, σ) plane at a frequency of 5 GHz. The sensitivity is expressed in logarithmic scale, that is, $\log_{10}(S_{\epsilon_m}^{\Gamma})$. As the figures illustrate, for a given relative permittivity ϵ_r , the sensitivity varies dramatically over the conductivity σ . However, for a fixed conductivity σ , changes in the medium relative permittivity ϵ_r have a smaller effect on the observed sensitivity. The conical probe with $\alpha = 70^\circ$ has the largest variation in sensitivity with a peak around $\sigma = 15$, and then drops sharply for higher conductivity values. The higher the cut angle α , the greater the regions in the graphs where the sensitivity is below zero (blue areas).

Fig. 9(a) and (b) compare the sensitivity of the analyzed geometries for two fixed values of conductivity, i.e., $\sigma = 0$ S/m and 10 S/m, respectively, at 5 GHz. These figures indicate that the flat probe ($\alpha = 0$) has a more consistent sensitivity over different values of ϵ_r than other geometries. Considering the sharp geometries, the conical probe with $\alpha = 70^\circ$ has better sensitivity for low values of ϵ_r and σ , while the bevelled probe with $\alpha = 60^\circ$ has higher sensitivity for high relative permittivity values. This suggests that bevelled probes have advantages over the conical probe in terms of sensitivity and resolution for tissue measurement. This is because biological tissues have high permittivity due to the high content of water. Since the sensitivity decreases with the cut angle α in high permittivity, there is a trade-off between probe sharpness and sensitivity for tissue measurement.

An implication of the sensitivity distribution over the (ϵ_r, σ) plane is how coaxial probes map these ϵ_r and σ values

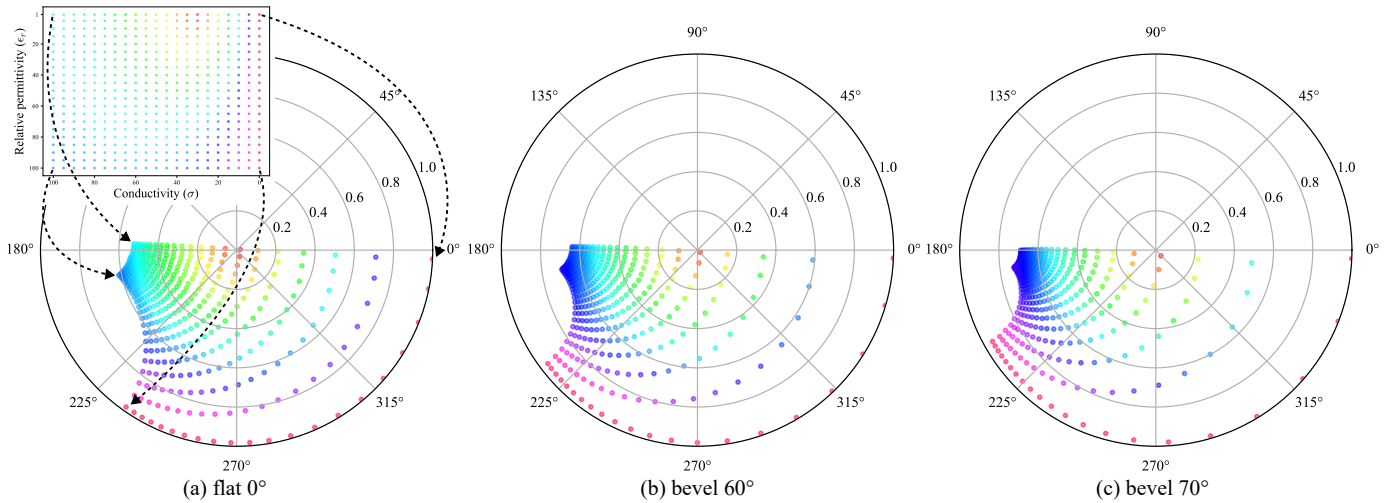


Fig. 10. Mapping of relative permittivity and conductivity (ϵ_r, σ) plane into reflection coefficient (Γ) plane by (a) flat, (b) bevelled 60° and (c) bevelled 70° coaxial probe at 10 GHz.

into the reflection coefficient plane, as shown in Fig. 10. The reflection coefficient plane represents the complex values (phase and magnitude) of the reflection coefficients (Γ) in polar coordinates. These are the reflection coefficients of flat and bevelled probes at 10 GHz used for training the model earlier. It is evident that for the same distanced values of the relative permittivity (ϵ_r) and conductivity (σ), the distances in the mapped reflection coefficient values decreased significantly for higher values of permittivity. This effect increases with the probe's cut angle; a phenomenon that was also observed by analysis of the model.

These results are consistent with the uncertainty analysis on flat open-ended coaxial probes conducted by Stuchly *et al.* [29]. One can conclude that increasing the cut angle or frequency, and changing the geometry from bevelled to conical (while maintaining the same cut angle) has a similar effect on the sensitivity as increasing the probe diameter. In other words, all these effects are equivalent to increasing the probe's aperture.

VI. CONCLUSION

A sensitivity analysis of two new probe geometries is performed in this paper using a model that incorporates the analytical solution of their aperture admittance. The presented model is accurate and only requires its coefficients to be calculated once for every probe geometry, via either simulation or experimental results. Experimental results conducted with a prototype probe confirmed the accuracy of the model.

The objective of sensitivity analysis is to find the geometry with the lowest uncertainty (i.e., highest sensitivity) within the permittivity range of biological tissues. As Fig. 8 illustrates, for all geometries high sensitivity is achieved for a limited range of permittivity. However, for a frequency between 500 MHz to 10 GHz, the relative permittivity (ϵ_r) of biological tissues ranges from 10 to 100, and the conductivity (σ) varies from 1 S/m to 10 S/m [2]. Within this range, the flat probe shows the best results with a sensitivity value of 1, while

amongst the sharp geometries, the 60° bevelled probe has the highest sensitivity, see Fig. 9 (b).

Compared to the bevelled probe, the sensitivity analysis shows that the conical probe is less accurate when distinguishing measurements obtained from tissue samples with similar dielectric values. The reduced sensitivity of the probe thus makes the classification more prone to measurement errors, and this phenomenon is amplified as the cutting angle increases.

The proposed probe geometries can cut through biological tissue and thus they can be easily integrated into surgical tools for real-time permittivity measurement of the tissue at the tooltip. Since other coaxial probes previously studied in the literature cannot cut through tissue, they are limited to *ex-vivo* measurements. *in-vivo* measurements have several advantages over *ex-vivo* measurements. Firstly, excised tissues may have different permittivity values than *in-vivo* because of lost water content, temperature change, etc.. This could easily lead to incorrect tissue classification. Secondly, real-time permittivity measurements of internal organs during diagnoses or treatment could increase the physicians' ability to correctly locate the target and, in case of focal therapy, result in a more concentrated treatment reducing damage to adjacent healthy tissues. The analyzed diameter of the two mentioned probe geometries makes it possible to integrate them into many medical monitoring tools and the model has shown satisfactory accuracy, especially in the range of permittivity values of most biological tissues.

REFERENCES

- [1] C. Gabriel, S. Gabriel, and y. E. Corthout, "The dielectric properties of biological tissues: I. literature survey," *Physics in medicine & biology*, vol. 41, no. 11, p. 2231, 1996.
- [2] S. Gabriel, R. Lau, and C. Gabriel, "The dielectric properties of biological tissues: Ii. measurements in the frequency range 10 hz to 20 ghz," *Physics in medicine & biology*, vol. 41, no. 11, p. 2251, 1996.
- [3] S. A. R. Naqvi, M. Manoufali, B. Mohammed, A. T. Mobashsher, D. Foong, and A. M. Abbosh, "In vivo human skin dielectric properties characterization and statistical analysis at frequencies from 1 to 30 ghz," *IEEE Transactions on Instrumentation and Measurement*, vol. 70, pp. 1–10, 2020.

- [4] H. Fallahi, J. Sebek, and P. Prakash, "Broadband dielectric properties of ex vivo bovine liver tissue characterized at ablative temperatures," *IEEE Transactions on Biomedical Engineering*, vol. 68, no. 1, pp. 90–98, 2020.
- [5] A. Fornes-Leal, N. Cardona, M. Frasson, S. Castell6-Palacios, A. Nevarez, V. P. Beltrán, and C. Garcia-Pardo, "Dielectric characterization of in vivo abdominal and thoracic tissues in the 0.5–26.5 ghz frequency band for wireless body area networks," *IEEE Access*, vol. 7, pp. 31 854–31 864, 2019.
- [6] R. Balduino, B. McDermott, E. Porter, M. A. Elahi, A. Shahzad, M. O'Halloran, and M. Cavagnaro, "Feasibility of water content-based dielectric characterisation of biological tissues using mixture models," *IEEE Transactions on Dielectrics and Electrical Insulation*, vol. 26, no. 1, pp. 187–193, 2019.
- [7] M. Hussein, F. Awwad, D. Jithin, H. El Hasasna, K. Athamneh, and R. Iratni, "Breast cancer cells exhibits specific dielectric signature in vitro using the open-ended coaxial probe technique from 200 mhz to 13.6 ghz," *Scientific reports*, vol. 9, no. 1, pp. 1–8, 2019.
- [8] R. J. Halter, A. Hartov, J. A. Heaney, K. D. Paulsen, and A. R. Schned, "Electrical impedance spectroscopy of the human prostate," *IEEE Transactions on Biomedical Engineering*, vol. 54, no. 7, pp. 1321–1327, 2007.
- [9] V. Mishra, A. Schned, A. Hartov, J. Heaney, J. Seigne, and R. Halter, "Electrical property sensing biopsy needle for prostate cancer detection," *The Prostate*, vol. 73, no. 15, pp. 1603–1613, 2013.
- [10] M. A. Stuchly and S. S. Stuchly, "Coaxial line reflection methods for measuring dielectric properties of biological substances at radio and microwave frequencies-a review," *IEEE Transactions on instrumentation and measurement*, vol. 29, no. 3, pp. 176–183, 1980.
- [11] J. R. Mosig, J.-C. E. Besson, M. Gex-Fabry, and F. E. Gardiol, "Reflection of an open-ended coaxial line and application to nondestructive measurement of materials," *IEEE Transactions on instrumentation and Measurement*, no. 1, pp. 46–51, 1981.
- [12] J. Grant, R. Clarke, G. Symm, and N. M. Spyrou, "A critical study of the open-ended coaxial line sensor technique for rf and microwave complex permittivity measurements," *Journal of Physics E: Scientific Instruments*, vol. 22, no. 9, p. 757, 1989.
- [13] D. Popovic, L. McCartney, C. Beasley, M. Lazebnik, M. Okoniewski, S. C. Hagness, and J. H. Booske, "Precision open-ended coaxial probes for in vivo and ex vivo dielectric spectroscopy of biological tissues at microwave frequencies," *IEEE Transactions on Microwave Theory and Techniques*, vol. 53, no. 5, pp. 1713–1722, 2005.
- [14] D. M. Hagl, D. Popovic, S. C. Hagness, J. H. Booske, and M. Okoniewski, "Sensing volume of open-ended coaxial probes for dielectric characterization of breast tissue at microwave frequencies," *IEEE Transactions on Microwave Theory and Techniques*, vol. 51, no. 4, pp. 1194–1206, 2003.
- [15] A. Mirbeik-Sabzevari and N. Tavassolian, "Characterization and validation of the slim-form open-ended coaxial probe for the dielectric characterization of biological tissues at millimeter-wave frequencies," *IEEE Microwave and Wireless Components Letters*, vol. 28, no. 1, pp. 85–87, 2017.
- [16] S. Halonen, J. Kari, P. Ahonen, K. Kronström, and J. Hyttinen, "Real-time bioimpedance-based biopsy needle can identify tissue type with high spatial accuracy," *Annals of biomedical engineering*, vol. 47, no. 3, pp. 836–851, 2019.
- [17] J. C. for Guides in Metrology (JCGM), "International vocabulary of metrology," no. 4, 2021. [Online]. Available: https://www.bipm.org/documents/20126/54295284/VIM4_CD_210111c.pdf
- [18] J. Anderson, C. Sibbald, and S. Stuchly, "Dielectric measurements using a rational function model," *IEEE transactions on microwave theory and techniques*, vol. 42, no. 2, pp. 199–204, 1994.
- [19] Y. Xu, R. Bosisio, A. Bonincontro, F. Pedone, and G. Mariutti, "On the measurement of microwave permittivity of biological samples using needle-type coaxial probes," *IEEE transactions on instrumentation and measurement*, vol. 42, no. 4, pp. 822–827, 1993.
- [20] D. M. Pozar, *Microwave engineering*. John wiley & sons, 2011.
- [21] D. V. Blackham and R. D. Pollard, "An improved technique for permittivity measurements using a coaxial probe," *IEEE Transactions on Instrumentation and Measurement*, vol. 46, no. 5, pp. 1093–1099, 1997.
- [22] M. G. Jushiddi, J. J. Mulvihill, D. Chovan, A. Mani, C. Shanahan, C. Silien, S. A. M. Tofail, and P. Tiernan, "Simulation of biopsy bevel-tipped needle insertion into soft-gel," *Computers in biology and medicine*, vol. 111, p. 103337, 2019.
- [23] B. Kent and C. Rossa, "Electric impedance spectroscopy feature extraction for tissue classification with electrode embedded surgical needles through a modified forward stepwise method," *Computers in Biology and Medicine*, vol. 135, p. 104522, 2021.
- [24] P. M. Meaney, A. P. Gregory, J. Seppälä, and T. Lahtinen, "Open-ended coaxial dielectric probe effective penetration depth determination," *IEEE transactions on microwave theory and techniques*, vol. 64, no. 3, pp. 915–923, 2016.
- [25] [Online]. Available: <http://www.netlib.org/lapack/>
- [26] D. P. Kingma and J. Ba, "Adam: A method for stochastic optimization," *arXiv preprint arXiv:1412.6980*, 2014.
- [27] A. P. Gregory and R. Clarke, "Tables of the complex permittivity of dielectric reference liquids at frequencies up to 5 ghz." 2012.
- [28] A. Nyshadham, C. L. Sibbald, and S. S. Stuchly, "Permittivity measurements using open-ended sensors and reference liquid calibration- an uncertainty analysis," *IEEE Transactions on Microwave Theory and Techniques*, vol. 40, no. 2, pp. 305–314, 1992.
- [29] S. Stuchly, C. Sibbald, and J. Anderson, "A new aperture admittance model for open-ended waveguides," *IEEE transactions on microwave theory and techniques*, vol. 42, no. 2, pp. 192–198, 1994.



Hossein Asilian Bidgoli is a Ph.D. student in System and Computer Engineering at Carleton University, Ottawa, Canada. He received the B.Sc. degree from Isfahan University of Technology, Isfahan, Iran, and the M.Sc. degree from Iran University of Science and Technology, Tehran, Iran, all in electrical engineering. His research interests include biomedical applications of microwave spectroscopy, electromagnetic parametric modelling and design, optimization algorithms, deep neural networks, and microwave circuits design and analysis.



Nicola Schieda is an abdominal radiologist at the Ottawa hospital and an Associate Professor in Radiology and Surgery at the University of Ottawa. He is the Director of Abdominal and Pelvic MRI and Prostate Imaging at the Ottawa hospital. He is a member of the Scientific Subcommittees for Genitourinary Imaging at the Radiological Society of North America, American Roentgen Ray Society and Society of Abdominal Radiology. He is a panel member of the American College of Radiology Appropriateness Criteria for Urological Imaging, a member of the Society of Abdominal Radiology Disease and is the Chair of the American College of Radiology Genitourinary Continuing Professional Improvement program. His current research interests include imaging of Genito-urinary malignancies and body MRI applications.



Carlos Rossa is an Associate Professor in the Department of Systems and Computer Engineering at Carleton University. He received his B.Eng. and M.Sc. degrees in Mechanical Engineering from the Ecole Nationale d'Ingénieurs de Metz, Metz, France, and earned his PhD degree in Mechatronics and Robotics from the Sorbonne Université (UPMC), Paris, France, under the auspices of the Commissariat à l'Energie Atomique (CEA). His research interests include biomedical instrumentation, medical robotics, and image-guided percutaneous surgery.